Interface Manipulation for Printing Three-Dimensional Microstructures Under Magnetic Guiding

*Libin Wang, Fengyu Li, Minuan Kuang, Meng Gao, Jingxia Wang, Yu Huang, Lei Jiang, and Yanlin Song**

3D microstructures[1,2] has aroused great interest and been applied in integrated electronics, tissue engineering, high-efficient collectors and sensors, photonic materials, etc.[3–6] Various 3D fabrication techniques have been proposed in decades, including self-assembly of in-plane units,[7,8] layer-by-layer printing,[9,10] direct writing,[11–14] and so on. Although these strategies provide flexible fabrication platform, the controllability of precise 3D microstructures remains a significant challenge. The fundamental problems involve the manipulation of the liquid wetting, dewetting,[15,16] coalescence,[17] transport,[18,19] and reshaping,[20,21] which influence the formation of the 3D architectures. Some efforts have been invested to control droplets by appropriate interface design. For instance, droplets were transformed to specific 3D microstructures based on pyroelectrodynamic-induced liquid–air interface deformation.[22,23] Moreover, externally driven magnetic droplets were separated into complicated pattern on superhydrophobic surfaces.[24] However, the relationship of 3D morphology and interfacial properties is still unclear, which limits the operability of droplets, resulting in poor 3D controllability. Hence, exploring the influence of interfacial properties upon final 3D morphology of printed droplets will have broad theoretical and technological implications.

Here we present a controllable strategy to print precise 3D microstructures via 2D interface manipulation of droplets on surfaces with tunable dynamic dewetting properties under magnetic guiding. For this purpose, a liquid–solid composite surface with tunable dynamic dewettability[25,26] and remarkable slip property[27,28] is constructed, where droplets possesses controllable stick-slip behavior and deformation performance. By tuning the dynamic dewettability, especially the receding angle of printed droplets on such surfaces, diverse 3D microstructures including hat, cone, pillar, and spindle are formed. The relationship between 3D morphology and interface properties is clarified. Accordingly, accurate-positioned and oriented-patterned 3D arrays are facilely printed, demonstrating high controllability and large-scale fabrication of uniform 3D microstructures. The as-prepared 3D microstructures and arrays have great potential in actuators,[29,30] sensors,[31,32] and phononic crystals study.[33] This advance in 3D fabrication technology based on interface manipulation will present significant insight and promising applications in controllable 3D manufacturing.

Figure 1a illustrates the scheme to achieve 3D microstructures on the liquid–solid composite surface guided by a cubic magnet. Magnetic ink (M-ink) droplets are printed onto the surface and deformed from hemispherical to pillared microstructure with droplet edge retracing. The orientation of the 3D microstructures can be altered within a wide tilting angle by deflecting the magnet, enabling asymmetric 3D manufacturing. The liquid–solid composite surface is constructed by swelling polydimethylsiloxane (PDMS) with silicone oil (Figure 1b). Swelling causes the PDMS chains to be unfolded and cladded of oil, forming a composite surface exposing a certain amount of liquid, which suppresses the resistance and favors the sliding of droplet. The dynamic dewettability of the surface can be accurately controlled by swelling ratio (defined as the ratio of absorbed silicone oil and PDMS), which essentially alternates the amount of liquid component (Figures S1a–c and S2, Supporting Information). Particularly, receding angle (θ_R) of the surface presents fine adjustability with the swelling ratio (Figure 1c). As a result, the M-ink droplets possess controllable retracing behavior (Figure S1d, Supporting Information). The formation scheme of the 3D microstructure is depicted in Figure 1d. Pulled by magnetic force F_m and distorted by resistance force F_r, the droplet is deformed into conic shape with fast reduced instantaneous contact angle (CA). When it is less than the receding angle, the droplet edge starts to retrace. With the droplet heightening and diameter reducing, the instantaneous CA increases gradually to reach the receding angle value and the raised droplet will not be drawn away due to the substrate resistance. Eventually, a 3D high-aspect-ratio microstructure is formed, and the base angle of the 3D structure on substrate is equal to its M-ink receding angle. A typical deformation process for one M-ink droplet on the composite surface with receding angle of *ca.* 95° was captured by a CCD-camera (Figure 1e). The dynamic evolutions show that the droplet is heightening

Dr. L. Wang, Dr. F. Li, Dr. M. Kuang, Dr. M. Gao, Dr. J. Wang, Dr. Y. Huang, Prof. L. Jiang, Prof. Y. Song
Beijing National Laboratory for Molecular Sciences (BNLMS)
Key Laboratory of Green Printing
Key Laboratory of Organic Solids
Institute of Chemistry Chinese Academy of Sciences
Beijing 100190, P. R. China
E-mail: ylsong@iccas.ac.cn
Dr. L. Wang, Dr. M. Kuang, Dr. M. Gao
School of Chemistry and Chemical Engineering
University of the Chinese Academy of Sciences
Beijing 100049, P. R. China

DOI: 10.1002/smll.201403355

www.MaterialsViews.com

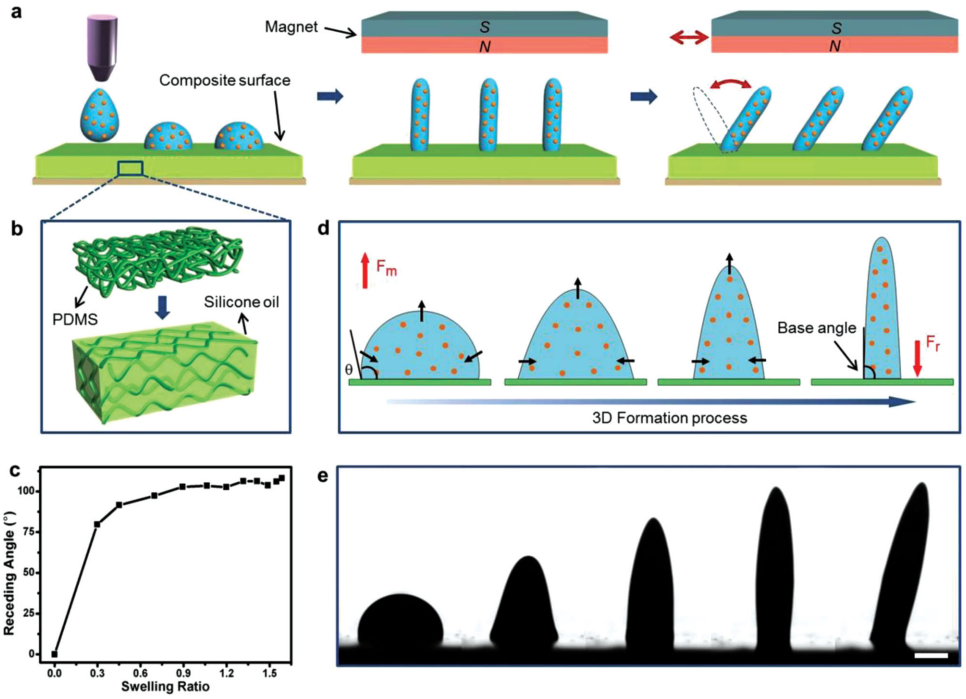

Figure 1. Interface manipulation principle for printing 3D microstructures. a) Schematic to achieve 3D microstructures by printing droplets on liquid–solid composite surface under magnet; the orientation of the microstructures can be controlled by magnetic guiding. b) Construction of the composite surface by swelling PDMS with silicone oil. c) Relevance of receding angle and swelling ratio of the surface, demonstrating tunable interface properties. d) Illustration of the droplet deformation and retraction process, which depends on the receding angle of the surface. e) Sequence of a pillar structure formed on swollen PDMS surface with receding angle of *ca.* 95°. Scale bar, 500 μm.

and its edge is retracing until the base angle approaches to around 90°, forming a 3D pillar structure. The corresponding shape parameter variation of diverse 3D microstructures on unswollen, partial-swollen and saturated-swollen PDMS with different receding angles were investigated, demonstrating various droplet retracing performances and controllable 3D morphologies (Figures S3, S4 and Movies S1–3, Supporting Information).

Figure 2 shows scanning electron microscopy (SEM) images of controlled 3D microstructures and printed arrays on different surfaces. On unswollen PDMS with large CA hysteresis and small receding angle ($\theta_R < 30°$), a hat-like 3D microstructure was obtained for the sticking of the droplet edge (Figure 2a). It has base angle of around 30°, and the base diameter approximate to that of the initially printed droplet of *ca.* 120 μm. Whereas, on the composite surfaces

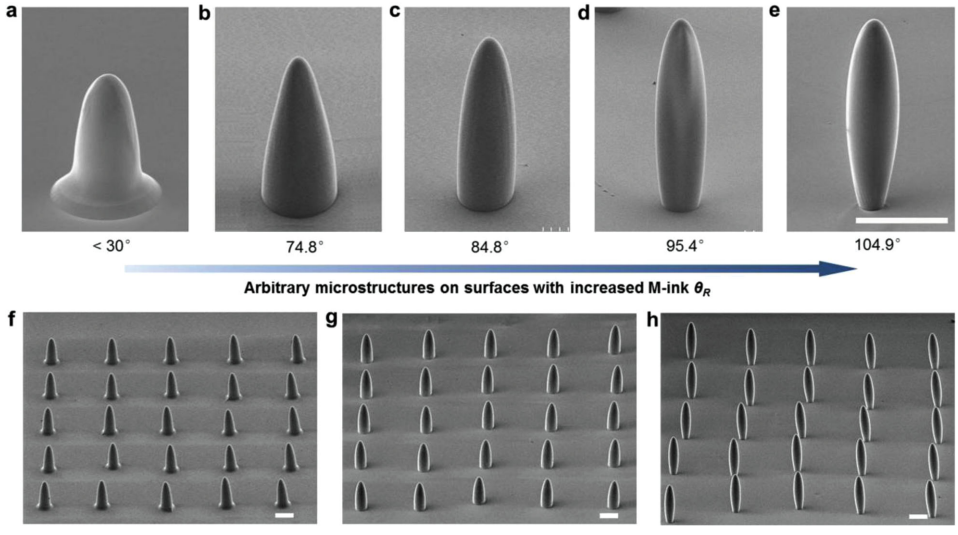

Figure 2. Controllability of 3D microstructures by inkjet printing on surfaces with tunable dewettability. a–e) Multiple microstructures shaped from hat, cone, and spindle on surfaces with increased M-ink receding angles. f) Hat array on unswollen PDMS with receding angle below 30°. g) Cone array on partial-swollen PDMS (swelling ratio of *ca.* 0.45) with receding angle of *ca.* 85°. h) Spindle array on saturated-swollen PDMS (swelling ratio of *ca.* 1.6) with receding angle beyond 90°. Scale bars, 100 μm; view angles, 60°.

small 2015,
DOI: 10.1002/smll.201403355

small NANO MICRO

of partial-swollen PDMS with M-ink θ_R of *ca.* 75°, 85°, and 95° (swelling ratios of *ca.* 0.29, 0.45, and 1.43), conic microstructures with different base angles and decreased diameters were generated due to the edge retraction of variant degrees (Figure 2b–d). Specifically, the 3D microstructures present pillared shape when θ_R is around 90°. As excessive sliding of the drop edge occurred on saturated-swollen PDMS (swelling ratio of *ca.* 1.6) with negligible CA hysteresis and large M-ink θ_R of *ca.* 105°, a spindle microstructure with base angle of about 105° was achieved (Figure 2e). The base and maximum middle diameter of the spindle is 28 μm and 49 μm, respectively. The SEM analysis shows that the interfacial dewetting properties directly influence the 3D morphology of the microstructures; indeed the base angle values correspond well with the receding angle values, and the diameters decrease with the enhancing of droplet retraction. Remarkably, typical 3D microstructure arrays of hat, cone, and spindle were easily prepared by inkjet printing (Figure 2f–h). Comparing to the irregular array consisted of random 3D microstructures on general surface (Figure S5, Supporting Information), the arrays prepared by interface manipulation on composite surfaces possess much more uniform 3D microstructures, achieving excellent controllability and large-scale fabrication for 3D printing technique.

As the receding angles of surfaces control the droplet retraction and the 3D morphologies, we illustrate the formation of typical 3D microstructures on the liquid–solid composite surfaces with different interfacial properties (**Figure 3**a). (i) On solid surface with extremely small receding angle (unswollen PDMS, $\theta_R < 30°$), the droplet is heightened but the edge can hardly retrace for the high interfacial resistance, deforming to hat-like structure. (ii) On liquid–solid composite surface with increased receding angle (partial-swollen PDMS with different swelling ratios), the droplet edge is retracing continuously because the decreased instantaneous CA can reach the receding angle readily. For receding angles ranging in 30°– 90°, the 3D structures possess conic configurations of serial base angles. Particularly, the 3D pillar structure can be obtained on surface with receding angle around 90°. (iii) On surface with receding angle approaching to its static CA (saturated-swollen PDMS, $\theta_R > 90°$), the droplet edge is easier to slide, thus spindle architecture is formed.

M-ink droplet presents elliptical deformation under the action of a perpendicular magnetic field (Figure S6, Supporting Information). The deformed droplet is subjected to both magnetic force F_m and resistance force F_r. Only if the magnetic force is not sufficient to overcome the resistance force $F_m \leq F_r$, stable 3D structures can be achieved without the whole droplet drawn away (gravity force is negligible for nanoliter droplets.[24] F_r is aligned with the vertical direction, whose value is related to the base diameter d of the 3D microstructure and the receding angle θ_R of the surface.[34] In this case, for constant magnetic force F_m acting on the jetted droplets,[35] the relevance of base diameter d and receding angle θ_R can be described as (details in Supporting Information)

$$d \geq 24.4/\sin\theta_R$$

Regarding the critical condition for available 3D microstructures, a curve corresponding to $d_c = 24.4/\sin\theta_R$ is presented (Figure 3b), where d_c suggests the critical base diameter of the 3D microstructures. In the experimented θ_R ranged from 0° to 90° on the composite PDMS surfaces, 3D structures show morphologies from hat to cone with decreased d_c. Particularly, high-aspect-ratio 3D microstructure can be achieved at receding angles around 90°. When θ_R is above 90°, 3D spindle structures would be obtained. For θ_R approaching 180°, the droplets tend to be drawn away due to their tiny surface resistance;[35] 3D microstructures with large d_c can only be obtained with mild droplet deformation and retraction. In Figure 3b, the green region predicts the feasible morphology (diameter and base angle) for 3D microstructures, while the pink region represents the parameter space where the droplet will be drawn away.

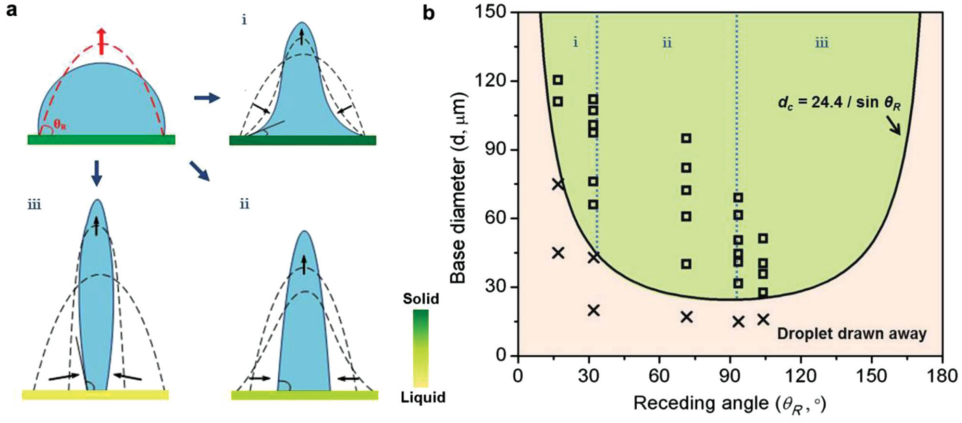

Figure 3. Interface manipulation sketch and capacity for printing desirable 3D microstructures. a) Models of typical 3D microstructures (i) hat, (ii) cone, and (iii) spindle formed on surfaces with different interfacial properties. b) Theoretical curve and experimental results predicting the morphology of the 3D microstructures. The solid curve shows the critical relevance between the base diameter of 3D microstructures and the receding angle of corresponding surfaces. The green region confines the feasible parameters for stable 3D microstructures, while the pink region indicates that the droplet would deviate or be drawn away. The squares and crosses represent the experimental results of available and unavailable 3D microstructures, respectively. The three regions separated by dotted lines correspond to the three typical 3D microstructures in a).

DOI: 10.1002/smll.201403355

To verify the analysis, we did statistics on the base diameters of the as-printed 3D microstructures and the receding angles of relevant surfaces. Controlled microstructure arrays can be prepared with parameter in the curve (squares in green region), while the 3D microstructures would either deviate from their designed positions or be drawn away as the magnetic force is larger than the resistance force (crosses in pink region, Figure S9, Supporting Information). The three regions separated by dotted lines correspond to the three typical 3D microstructures in Figure 3a, which are defined as hat, cone, and spindle. Manipulating the droplet retraction and deformation by tuning the 2D interfacial properties leads to diverse 3D microstructures, and the explored relevance between 3D morphology and dynamic dewettability of surface makes it possible to precisely design and control arbitrary 3D microstructures.

Interestingly, this strategy also allows versatile fabrication of asymmetric microstructures at a variety of tilting angles, paving the way to manufacture a wide palette of complex 3D microstructures. These tilted microstructures are created by laterally moving and rotating the magnet; the orientation and tilting angle of the resulted 3D microstructures correspond to the direction and displacements of the magnet (**Figure 4**a and Movie S4, Supporting Information). The tilted pillar microstructure is affected by both the magnetic force and the resistance force. Only if the resistance force is stronger than the magnetic force, the pillar droplet is inclined by a magnetic anisotropic torque without slipping on the surface. As a result, tilted 3D microstructures of diverse features and tilting angles were obtained (Figure 4b–e). Moreover, synchronized-tilted pillar arrays with certain angles were facilely printed (Figure 4f and Figure S10, Supporting Information). An anisotropic-tilted pillar row possessed tilting angles from 0° to 90° was achieved by rotating the magnet (Figure 4g).

In summary, manipulation of interfacial properties advances the capability of 3D construction by enabling controlled retraction and deformation of printed droplets. We have verified the relevance of interfacial properties and spatial microstructure parameters, and demonstrated that the 3D morphology is deterministically dependent on the dynamic dewettability of surface. Accordingly, precise control on the base angle, diameter and height of the 3D architectures was accomplished *via* managing the receding angles of surfaces, resulting in hat, cone, pillar, and spindle microstructures. Besides, more complex 3D morphologies can be attained by anisotropic interface manipulation of droplets (Figure S11, Supporting Information), for example, on patterned surface with differential dewettability. We have also fabricated patterned and asymmetric 3D microstructure arrays by inkjet printing under magnetic guiding, which enables versatile and large-scale 3D construction. As a general approach, numerous tunable interfaces could be adopted to satisfy the control of various inks (water, oil or solvents). Moreover, other triggers, such as electric field, capillary force, and thermo stimuli, can guide the deformation of droplets, offering a wide range of tools to fabricate diverse 3D microstructures. Furthermore, 3D microstructures with desired morphologies and elaborate optical/electrical properties could be achieved by developing functional materials as ink, providing this approach a promising future for on-demand and highly precise 3D manufacturing.

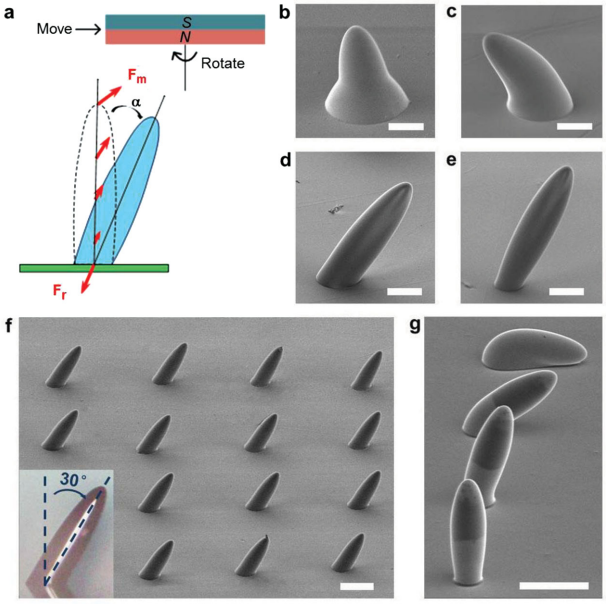

Figure 4. Versatile printing of asymmetric 3D microstructures. a) Schematic illustration of the force situation for a tilted pillar under deflecting magnetic field. SEM images of tilted b) hat; c) cone; d) pillar; and e) spindle with different tilting angles and orientations. Scale bars, 50 μm. f) Printed deflective pillar array with an accordant tilting angle of 30°. Insert is the optical micrograph of a pillar with view angle of 90°. g) An anisotropic-tilted pillar row by rotating the magnetic field in plane. Scale bars, 100 μm. All SEM view angles, 60°.

Experimental Section

M-Ink: Magnetic ink (M-ink) in this work was obtained by mixing ferrofluid (Beijing Shenran Tech. Co., Ltd., MFW), aqueous polyvinylalcohol (PVA 1788, Aladdin-reagent) solution of 10 wt%, and ethylene glycol (EG) with proportion of 1:0.4:0.6. It contained 17 wt% Fe_3O_4 nanoparticles with diameter below 10 nm. The surface tension and saturation magnetization were 52.37 ± 0.026 mN m^{-1} and *ca.* 100 ± 10 Gs, respectively.

Composite Surfaces: Liquid–solid composite surfaces with tunable dynamic dewettability were prepared from PDMS elastomer kits (Dow Corning Sylgard 184, 30: 1 precursor and curing agent) swollen by silicone oil (Shin-Etsu Chemical Industry Co., Ltd., Japan, KF-5, 5 cs). PDMS were spin-coated on cleaned glass slides, annealed at 80 °C for 1 h and then immersed in silicone oil for predetermined periods. After wiping excess oil on the surface, the swollen PDMS with different swelling ratios were used as tunable composite surfaces. In this work, swelling ratio was defined as the ratio of absorbed silicone oil and PDMS, and was measured by weighing PDMS at different swelling time.

The tunable dynamic dewetting properties of swollen PMDS were characterized by a contact angle (CA) measurement device (OCA20, DataPhysics, Germany) at 23 °C. Advancing angle and receding angle (θ_A and θ_R) were measured as 3 μL liquid was added and withdrawn dynamically from a surface-bound droplet. Contact angle hysteresis ($\Delta\theta$) was defined as the difference of advancing

DOI: 10.1002/smll.201403355

and receding angle. Sliding angle (α) was recorded by measuring the tilting of substrate for the movement of a 5 μL droplet on it. Each angle data was an average of at least five independent measurements on different positions of the same sample. More detailed data are shown in Figure S1, Supporting Information.

Printing Droplets: We printed the M-ink droplets onto the as-prepared composite surface by a jet printing system using the piezoelectric valve with dispensing volume of 2 nL (PicoDot EFD, Nordson, USA). A cubic NdFeB magnet was placed vertically upon the droplets without touching them, inducing the droplet to deform and retrace on the surface to generate freestanding 3D microstructures. The position and movement of droplets and arrays were accurately controlled by 4-axis stepping motors with positioning accuracy of 1 μm (JR2200N Desktop Robot, Nordson, USA).

Magnet and Magnetic Field: A cubic NdFeB permanent magnet with size of $5 \times 2.5 \times 5$ cm^3 was used. Magnetic field intensity (H) was measured as a function of the distance from the surface of the magnet by a Gauss meter (Digital Measurement System SG-3M, China). Vertical magnetic field gradient (grad H) was obtained from the derivation of the measured magnetic field intensity. Detailed data are shown in Figure S8, Supporting Information.

Characterization: The morphologies of the 3D microstructures were characterized by a field-emission scanning electron microscope (SEM, JEOL, JSM-7500F, Japan). All the SEM photographs were taken at a view angle of 60° unless stated. The droplet deformation process was acquired by a CCD-camera with capture speed of 25 frame s^{-1} and resolution of 768×576 pixel^2 equipped of a white-light-emitting lamp and a zooming lens (SCA40, Dataphysics, Germany).

Supporting Information

Supporting Information is available from the Wiley Online Library or from the author.

Acknowledgements

The authors thank the financial support by the National Nature Science Foundation (Grant Nos. 51173190 and 21121001), the 973 Program (Nos. 2013CB933004, 2011CB932303, and 2011CB808400), and the "Strategic Priority Research Program" of the Chinese Academy of Sciences (Grant No. XDA09020000).

[1] B. Derby, *Science* **2012**, *338*, 921.
[2] B. Y. Ahn, E. B. Duoss, M. J. Motala, X. Guo, S. I. Park, Y. Xiong, J. Yoon, R. G. Nuzzo, J. A. Rogers, J. A. Lewis, *Science* **2009**, *323*, 1590.
[3] R. Galland, P. Leduc, C. Guérin, D. Peyrade, L. Blanchoin, M. Théry, *Nat. Mater.* **2013**, *12*, 416.
[4] D. B. Kolesky, R. L. Truby, A. S. Gladman, T. A. Busbee, K. A. Homan, J. A. Lewis, *Adv. Mater.* **2014**, *26*, 3124.
[5] K. Li, J. Ju, Z. Xue, J. Ma, L. Feng, S. Gao, L. Jiang, *Nat. Commun.* **2013**, *4*, 2276.
[6] K. Aoki, H. T. Miyazaki, H. Hirayama, K. Inoshita, T. Baba, K. Sakoda, N. Shinya, Y. Aoyagi, *Nat. Mater.* **2003**, *2*, 117.
[7] M. Boncheva, S. A. Andreev, L. Mahadevan, A. Winkleman, D. R. Reichman, M. G. Prentiss, S. Whitesides, G. M. Whitesides, *Proc. Natl Acad. Sci. U.S.A.* **2005**, *102*, 3924.
[8] M. Jamal, A. M. Zarafshar, D. H. Gracias, *Nat. Commun.* **2011**, *2*, 527.
[9] P. Galliker, J. Schneider, H. Eghlidi, S. Kress, V. Sandoghdar, D. Poulikakos, *Nat. Commun.* **2012**, *3*, 890.
[10] G. Villar, A. D. Graham, H. Bayley, *Science* **2013**, *340*, 48.
[11] G. M. Gratson, M. J. Xu, J. A. Lewis, *Nature* **2004**, *428*, 386.
[12] K. Sun, T. S. Wei, B. Y. Ahn, J. Y. Seo, S. J. Dillon, J. A. Lewis, *Adv. Mater.* **2013**, *25*, 4539.
[13] C. Ladd, J. H. So, J. Muth, M. D. Dickey, *Adv. Mater.* **2013**, *25*, 4953.
[14] J. T. Kim, S. K. Seol, J. Pyo, J. S. Lee, J. H. Je, G. Margaritondo, *Adv. Mater.* **2011**, *23*, 1968.
[15] Y. Y. Noh, N. Zhao, M. Caironi, H. Sirringhause, *Nat. Nanotechnol.* **2007**, *2*, 784.
[16] M. Caironi, E. Gili, T. Sakanoue, X. Cheng, H. Sirringhaus, *ACS Nano* **2010**, *4*, 1451.
[17] T. Wauer, H. Gerlach, S. Mantri, J. Hill, H. Bayley, K. Tanuj Sapra, *ACS Nano* **2014**, *8*, 771.
[18] H. Mertaniemi, R. Forchheimer, O. Ikkala, R. H. A. Ras, *Adv. Mater.* **2012**, *24*, 5738.
[19] P. Aussillous, D. Quéré, *Nature* **2001**, *411*, 924.
[20] K. Piroird, B. D. Texier, C. Clanet, D. Quéré, *Phys. Fluids* **2013**, *25*, 032108.
[21] J. J. Balowski, Y. Wang, N. L. Allbritton, *Adv. Mater.* **2013**, *25*, 4107.
[22] P. Ferraro, S. Coppola, S. Grilli, M. Paturzo, V. Vespini, *Nat. Nanotechnol.* **2010**, *5*, 429.
[23] S. Grilli, S. Coppola, V. Vespini, F. Merola, A. Finizio, P. Ferraro, *Proc. Natl Acad. Sci. USA* **2011**, *108*, 15106.
[24] J. V. I. Timonen, M. Latikka, L. Leibler, R. H. A. Ras, O. Ikkala, *Science* **2013**, *341*, 253.
[25] T.-S. Wong, S. H. Kang, S. K. Y. Tang, E. J. Smythev B. D. Hatton, A. Grinthal, J. Aizenberg, *Nature* **2011**, *477*, 443.
[26] X. Yao, Y. Hu, A. Grinthal, T.-S. Wong, L. Mahadevan, J. Aizenberg, *Nat. Mater.* **2013**, *12*, 529.
[27] N. Vogel, R. A. Belisle, B. Hatton, T. S. Wong, J. Aizenberg, *Nat. Commun.* **2013**, *4*, 2176.
[28] A. Lafuma, D. Quéré, *Europhys. Lett.* **2011**, *96*, 56001.
[29] J. Belardi, N. Schorr, O. Prucker, J. Rühe, *Adv. Funct. Mater.* **2011**, *21*, 3314.
[30] D. Wu, S.-Z Wu, S. Zhao, J. Yao, J.-N. Wang, Q.-D. Chen, H.-B. Sun, *Small* **2013**, *9*, 760.
[31] E. P. Gnanamanickam, J. P Sullivan, *J. Micromech. Microeng* **2012**, *22*, 125015.
[32] J. Digabel, N. Biais, J. Fresnais, J.-F. Berret, P. Hersen, B. Ladoux, *Lab Chip* **2011**, *11*, 2630.
[33] Y. Pennec, J. O. Vasseur, B. Djafari-Rouhani, L. Dobrzyński, P. A. Deymierb, *Surf. Sci. Rep.* **2010**, *65*, 229.
[34] N. Havard, F. Risso, Ph. Tordjeman, *Phys. Rev. E* **2013**, *88*, 013014.
[35] J. V. I. Timonen, M. Latikka, O. Ikkala, R. H. A. Ras, *Nat. Commun.* **2013**, *4*, 2398.

Received: November 12, 2014
Published online: